INORGANIC CHEMISTRY
FRONTIERS

RESEARCH ARTICLE

View Article Online
View Journal | View Issue

Cite this: *Inorg. Chem. Front.*, 2017, **4**, 171

Anion-driven tetrel bond-induced engineering of lead(II) architectures with *N*′-(1-(2-pyridyl)ethylidene)nicotinohydrazide: experimental and theoretical findings†

Ghodrat Mahmoudi,*[a] Damir A. Safin,*[b] Mariusz P. Mitoraj,*[c] Mojtaba Amini,*[a] Maciej Kubicki,[d] Thomas Doert,[e] Franziska Locherer[e] and Michel Fleck[f]

Received 2nd November 2016,
Accepted 24th November 2016

DOI: 10.1039/c6qi00477f

rsc.li/frontiers-inorganic

The evaluation of *N*′-(1-(2-pyridyl)ethylidene)nicotinohydrazide (**HL**) as a linker for the Pb^{II} tagged extended structures is described. The reaction of $Pb(ClO_4)_2$ or $Pb(OAc)_2$ with **HL** in MeOH at 60 °C and room temperature, respectively, leads to heteroleptic complexes **{[PbL]ClO$_4$}$_n$·nH$_2$O** and **[PbL(OAc)]$_2$**, while the same reaction of $Pb(ClO_4)_2$ with **HL** at 60 °C in the presence of two equivalents of NaOAc or $NaNO_2$ leads to heteroleptic complexes **{[Pb(HL)(OAc)]ClO$_4$}$_n$** and **[PbL(NO$_2$)]$_n$**, respectively. Using $Pb(NO_3)_2$ as a source of Pb^{II} in the same reaction with **HL** and two equivalents of NaN_3 or NaNCS at room temperature yields **[PbLN$_3$]$_n$** and **[Pb$_2$(HL)$_2$(NO$_3$)$_2$(NCS)$_2$]**, respectively. The room temperature reaction of $Pb(NO_3)_2$ with **HL** in the presence of two equivalents of $NaClO_4$ leads to the transformation of the parent ligand to its perchlorate salt **[H$_2$L]ClO$_4$**. In all the obtained Pb^{II} structures, **HL** or its deprotonated form **L** acts both as a chelating and a bridging ligand. The nature of the inorganic anion also influences the final structure. In all complexes the Pb^{II} center exhibits a hemidirected coordination geometry with all the covalent bonds being concentrated on one hemisphere of the coordination sphere with the closest approach of two atoms on the other side varying from 151° to 232°. The sterically available Pb^{II} ion participates in tetrel bonding as evidenced from the detailed structural analysis of the described complexes. As a result of tetrel bonding, the structures of all the six compounds can be extended to a higher dimensional framework, which is further stabilized by π···π stacking interactions between the aromatic rings. The DFT based charge and energy decomposition (ETS-NOCV) calculations are performed in order to shed light on the nature of non-covalent interactions that determine the stability of the obtained structures.

Introduction

In recent years metal–organic supramolecular systems have attracted great interest for their extremely versatile coordination motifs and potential applications as functional materials in numerous and diverse fields including separation, drug delivery, catalysis, molecular magnetism, gas adsorption and photoluminescence.[1–21] The development of new synthetic strategies to produce metal–organic frameworks (MOFs) and coordination polymers (CPs) has become a great challenge because it depends on many factors such as the nature of the metal ion and its counter ion, structural features of the organic ligand and experimental conditions (reaction temperature, reagent ratio, pH, solvent(s)), and crystallization procedures.[22–26] Furthermore, among the most powerful tools to design and control the structure of supramolecular systems, non-covalent inter- and intramolecular interactions are the most efficient. Non-covalent interactions play pivotal roles in

[a]*Department of Chemistry, Faculty of Science, University of Maragheh, P.O. Box 55181-83111, Maragheh, Iran. E-mail: mahmoudi_ghodrat@yahoo.co.uk, mamini@maragheh.ac.ir*
[b]*Institute of Condensed Matter and Nanosciences, Molecules, Solids and Reactivity (IMCN/MOST), Université catholique de Louvain, Place L. Pasteur 1, 1348 Louvain-la-Neuve, Belgium. E-mail: damir.a.safin@gmail.com*
[c]*Department of Theoretical Chemistry, Faculty of Chemistry, Jagiellonian University, R. Ingardena 3, 30-060 Cracow, Poland. E-mail: mitoraj@chemia.uj.edu.pl*
[d]*Faculty of Chemistry, Adam Mickiewicz University in Poznan, Umultowska 89b, 61-614 Poznan, Poland*
[e]*Department of Chemistry and Food Chemistry, Dresden University of Technology, Helmholtzstrasse 10, 01069 Dresden, Germany*
[f]*Institute for Mineralogy and Crystallography, University of Vienna, Althanstrasse 14, 1090 Vienna, Austria*

†Electronic supplementary information (ESI) available: Fig. S1–S7 and cif files. CCDC 1059556–1059562. For ESI and crystallographic data in CIF or other electronic format see DOI: 10.1039/c6qi00477f

many aspects of chemistry and biology, with van der Waals interactions and hydrogen bonding being among the best known examples. Nowadays the construction of any host to bind guest species is possible thanks to modern synthetic chemistry methods even in competitive media.[27,28]

A more recently defined class of non-covalent interactions, that continues to garner a significant degree of attention, are classified as σ-hole bonds, *i.e.* interactions between a covalently-bonded atom of groups IV–VII acting as a Lewis acid and a Lewis base centre.[29–32] σ-Hole bonding is a primarily electrostatic interaction between a localized region of positive electrostatic potential (ESP) on a molecular species (the σ-hole) and an electron-rich center nearby. Among σ-hole bonds, halogen,[33–41] chalcogen[42–50] and pnictogen[51–53] interactions are the most studied bonds, where atoms of groups VII, VI and V, respectively, act as Lewis acid centres. More recently atoms of the group IV have also been considered as Lewis acid centres forming σ-hole bonds.[32,54–62] The σ-hole bond formed by the group IV elements has been named a tetrel bond.[55,59]

Intrigued by this new class of σ-hole bonding, *i.e.* the tetrel bond, we have recently directed our attention towards Pb^{II},[63–66] as a perfect template for the formation of tetrel bonds. Particularly, lead is the heaviest group IV element and thus can be expected to form more positive σ-holes than other elements of this group. Furthermore, the experimental coordination geometry around lead, reveals two distinct structural features, namely holodirected, in which the bonds to ligand atoms are directed throughout the surface of the encompassing globe, and hemidirected, in which the bonds to ligand atoms are directed throughout only part of the globe, that is, there is an identifiable void (or gap) in the distribution of bonds to the ligands (Chart 1).[67,68] While all Pb^{IV} compounds show a holodirected coordination geometry, for Pb^{II} both holodirected and hemidirected coordination geometries are found.[67] A hemidirected coordination geometry around Pb^{II}, with a pronounced gap in the coordination sphere, would substantially facilitate closer approach of electron donors to the σ-hole of the Pb^{II} ion than to those of the other group IV atoms and thus enable the formation of a stronger tetrel bond with a more predictable geometry.

In this work we have been continuing our comprehensive investigations toward the synthesis of new Pb^{II} containing supramolecular assemblies driven by non-covalent interactions. Namely, we report for the first time that depending on the temperature a reaction of *N′*-(1-(2-pyridyl)ethylidene)nicotinohydrazide (**HL**)[69] with Pb^{II} salts, comprising a wide set of anions that differ structurally (NO_2^-, NO_3^-, ClO_4^-, N_3^-, NCS^- and OAc^-), yields either a new perchlorate salt $\mathbf{[H_2L]ClO_4}$ of a helice-like structure, or new Pb^{II} structures with intriguing architectures including, *e.g.*, a very rare example of $Pb^{II}\cdots Pb^{II}$ interaction.

The structure of the ligand is designed with the potential to form tridentate chelation of one metal center, with a meridional N_2O coordination motif analogous to the classical 2,2′:6′,2″-terpyridine or bis(imino)pyridine ligands,[70,71] while the remaining nitrogen atom of the 3-pyridyl fragment remains free to bind to another metal center, forming a bridge and leading to either di- or polymeric coordination compounds. The polydentate nature of both the ligand **HL** and its conjugate anion **L** facilitates the hemidirected coordination of Pb^{II}, while the nature of inorganic anions ensures the presence of electron donor atoms capable of forming tetrel bonds. Indeed, in the crystal structures of all the reported herein Pb^{II} complexes, tetrel bonds with hemidirected coordination spheres of the metal ions are mainly responsible for the formation of 3D supramolecular aggregates. The nature of non-covalent interactions in all the structures was studied for the first time by the DFT based charge and energy decomposition calculations (ETS-NOCV).

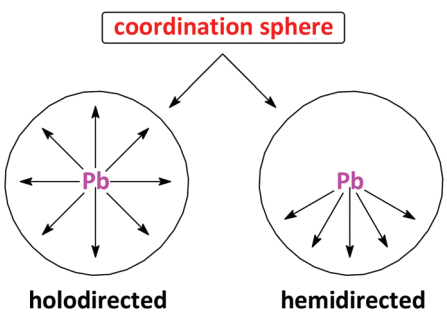

Chart 1 The simplified diagram of the holodirected and hemidirected coordination spheres around lead.

Results and discussion

An equimolar one-pot reaction of $Pb(ClO_4)_2$ or $Pb(OAc)_2$ with **HL** in MeOH at 60 °C and room temperature, respectively, leads to heteroleptic complexes $\mathbf{\{[PbL]ClO_4\}_n\cdot nH_2O}$ and $\mathbf{[PbL(OAc)]_2}$, each containing the deprotonated form of the organic ligand **L** (Scheme 1). The same reaction of $Pb(ClO_4)_2$ with **HL** at 60 °C but in the presence of two equivalents of NaOAc or $NaNO_2$ also leads to heteroleptic complexes $\mathbf{\{[Pb(HL)(OAc)]ClO_4\}_n}$ and $\mathbf{[PbL(NO_2)]_n}$, respectively (Scheme 1). While the latter structure is also constructed from the deprotonated ligand **L**, the former compound, however, contains the parent ligand in its neutral form **HL**. Using $Pb(NO_3)_2$ as a source of Pb^{II} in the same reaction with **HL** and two equivalents of NaN_3 or NaNCS at room temperature yields $\mathbf{[PbLN_3]_n}$ and $\mathbf{[Pb_2(HL)_2(NO_3)_2(NCS)_2]}$, respectively (Scheme 1). Interestingly, the room temperature reaction of $Pb(NO_3)_2$ with **HL** in the presence of two equivalents of $NaClO_4$ leads to the transformation of the parent ligand to its perchlorate salt $\mathbf{[H_2L]ClO_4}$ (Scheme 1).

All compounds were obtained with good yields, and were fully characterized by elemental analysis, FTIR spectroscopy, single crystal X-ray diffraction and theoretical calculations.

According to the single crystal X-ray diffraction data, $\mathbf{\{[PbL]ClO_4\}_n\cdot nH_2O}$ and $\mathbf{[Pb_2(HL)_2(NO_3)_2(NCS)_2]}$ crystallize in the monoclinic space group $P2_1/n$, while $\mathbf{[PbL(NO_2)]_n}$, $\mathbf{[H_2L]ClO_4}$ and $\mathbf{[PbL(OAc)]_2}$ crystallize in the monoclinic space group

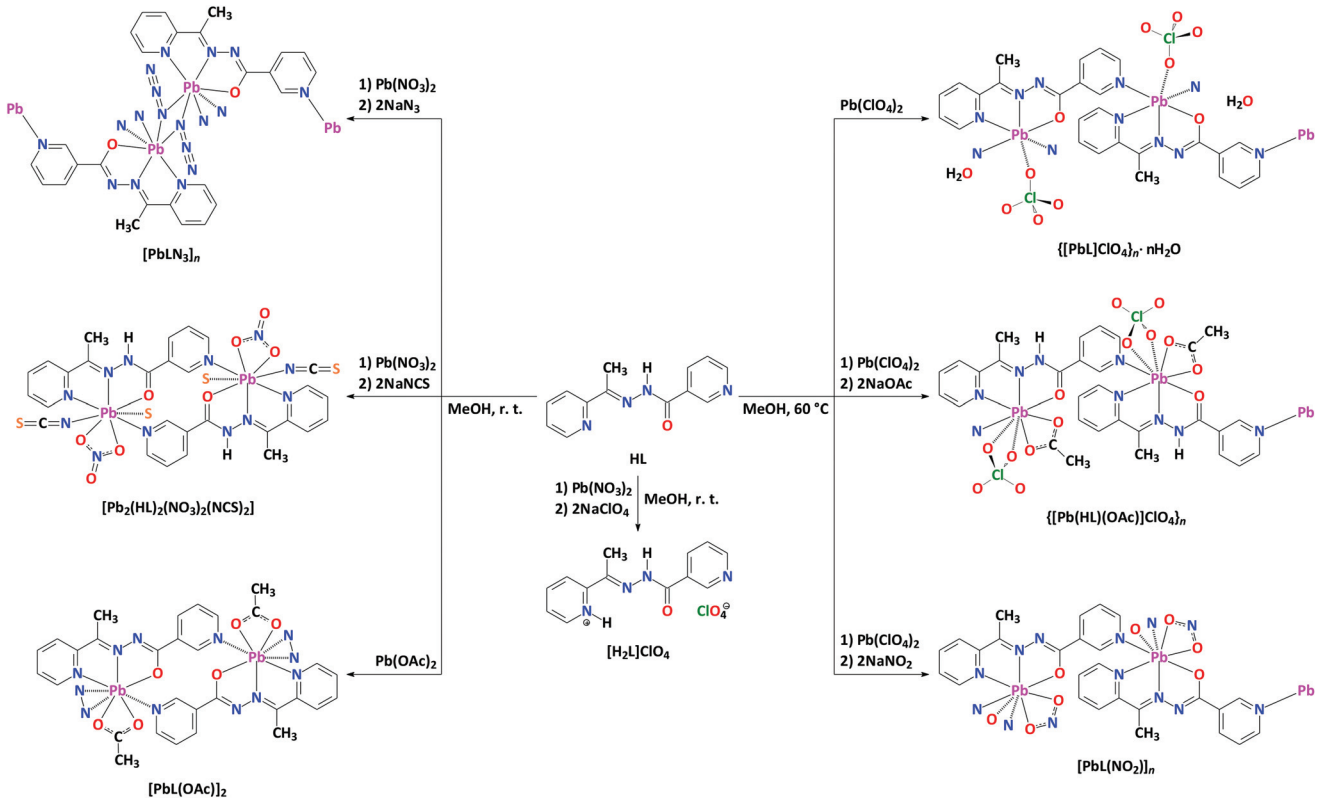

Scheme 1 Syntheses of $[H_2L]ClO_4$ and Pb^{II} complexes described in this work. Tetrel bonds are shown as dashed lines.

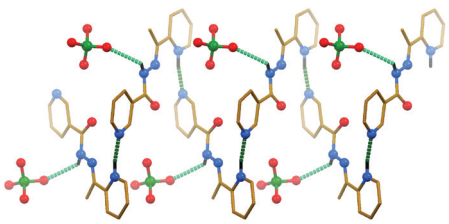

Fig. 1 Left handed helix, constructed through hydrogen bonds, in the crystal structure of $[H_2L]ClO_4$ (CH hydrogen atoms are omitted for clarity). Hydrogen bonds are shown as dashed lines. Stronger non-covalent interactions are shown in a darker shade of green than the weaker non-covalent interactions. Color code: C = gold, H = black, N = blue, Cl = green, O = red.

$P2_1/c$, respectively. Compound $\{[Pb(HL)(OAc)]ClO_4\}_n$ crystallizes in the orthorhombic space group *Pbca*, while the complex $[PbLN_3]_n$ crystallizes in the triclinic space group $P\bar{1}$.

The ligand cation in the structure of $[H_2L]ClO_4$ is almost flat (Fig. 1) and the dihedral angle between the mean planes of rings is 9.9(4)°. The bond length and angles establish the double-bond character of the N–C(CH_3) bond (1.266(10) Å). The protonation nitrogen site of the 2-pyridyl ring is confirmed by the localization of the hydrogen atom in the difference Fourier map and the successful refinement of this atom and the bond angles pattern around the nitrogen atom. In the crystal structure of $[H_2L]ClO_4$ the ligand cations are linked through intermolecular N–H···N hydrogen bonds (Table 1), formed between the pyridinium NH hydrogen atom of one cation and the nitrogen atom of the 3-pyridyl fragment of an adjacent cation. As a result of these interactions, left and right handed helices are formed (Fig. 1). Furthermore, the amide NH hydrogen atom of the ligand cation is involved in the intermolecular N–H···O hydrogen bond with one of the oxygen atoms of an adjacent ClO_4^- anion (Fig. 1 and Table 1). The

Table 1 Classic hydrogen bond lengths (Å) and angles (°) for $[H_2L]ClO_4$, $\{[Pb(HL)(OAc)]ClO_4\}_n$ and $[Pb_2(HL)_2(NO_3)_2(NCS)_2]$

Compound	D–H···A	*d*(D–H)	*d*(H···A)	*d*(D···A)	∠(DHA)
$[H_2L]ClO_4$ [a]	N(8A)–H(8A)···O(3B)$^{\#1}$	0.92	2.47	3.085(11)	125
	N(12A)–H(12A)···N(1A)$^{\#2}$	0.98	1.82	2.752(9)	158
$\{[Pb(HL)(OAc)]ClO_4\}_n$ [b]	N(8A)–H(8A)···O(11B)$^{\#1}$	0.88	2.15	2.923(7)	146
$[Pb_2(HL)_2(NO_3)_2(NCS)_2]$ [c]	N(8A)–H(8A)···O(2C)$^{\#1}$	0.88	2.18	2.961(3)	147

[a] Symmetry transformations used to generate equivalent atoms: #1 $x, -1+y, z$; #2 $1-x, 1/2+y, 1/2-z$. [b] Symmetry transformations used to generate equivalent atoms: #1 $1-x, 1-y, 1-z$. [c] Symmetry transformations used to generate equivalent atoms: #1 $1/2-x, -1/2+y, 1/2-z$.

Table 2 π···π distances (Å) and angles (°) for $[H_2L]ClO_4$ and Pb^{II} complexes described in this work[a]

Compound	Cg(*I*)	Cg(*J*)	*d*[Cg(*I*)–Cg(*J*)]	*α*	*β*	*γ*	Slippage
$[H_2L]ClO_4$ [b]	Cg(1)	Cg(2)$^{\#1}$	3.757(5)	9.9(4)	21.8	22.9	1.394
	Cg(2)	Cg(1)$^{\#2}$	3.756(5)	9.9(4)	22.9	21.8	1.463
$\{[PbL]ClO_4\}_n \cdot nH_2O$ [c]	Cg(4)	Cg(5)$^{\#1}$	3.675(3)	11.6(3)	25.0	19.4	1.555
	Cg(5)	Cg(4)$^{\#1}$	3.675(3)	11.6(3)	19.4	25.0	1.223
$\{[Pb(HL)(OAc)]ClO_4\}_n$ [d]	Cg(1)	Cg(2)$^{\#1}$	3.694(5)	8.7(4)	25.6	18.6	1.595
	Cg(2)	Cg(1)$^{\#1}$	3.695(5)	8.7(4)	18.6	25.6	1.179
$[PbL(NO_2)]_n$ [e]	Cg(4)	Cg(4)$^{\#1}$	3.615(3)	0.0(3)	26.0	26.0	1.586
$[PbLN_3]_n$ [f]	Cg(4)	Cg(5)$^{\#1}$	3.930(3)	12.0(2)	20.1	32.0	1.348
	Cg(4)	Cg(5)$^{\#2}$	3.809(3)	12.0(2)	20.4	22.8	1.325
	Cg(5)	Cg(4)$^{\#3}$	3.809(3)	12.0(2)	22.8	20.4	1.478
	Cg(5)	Cg(4)$^{\#4}$	3.930(3)	12.0(2)	32.0	20.1	2.085
$[Pb_2(HL)_2(NO_3)_2(NCS)_2]$ [g]	Cg(1)	Cg(2)$^{\#1}$	3.7404(19)	14.76(16)	7.7	10.6	0.499
	Cg(1)	Cg(2)$^{\#2}$	3.7947(19)	5.02(16)	27.1	22.9	1.729
	Cg(2)	Cg(1)$^{\#3}$	3.7404(19)	14.76(16)	10.6	7.7	0.689
	Cg(2)	Cg(1)$^{\#2}$	3.7948(19)	5.02(16)	22.9	27.1	1.477
$[PbL(OAc)]_2$ [h]	Cg(1)	Cg(2)$^{\#1}$	3.839(3)	10.7(2)	20.0	30.7	1.313
	Cg(2)	Cg(1)$^{\#1}$	3.839(3)	10.7(2)	30.7	20.0	1.960

[a] Cg(*I*)–Cg(*J*): distance between ring centroids; *α*: dihedral angle between planes Cg(*I*) and Cg(*J*); *β*: angle Cg(*I*) → Cg(*J*) vector and normal to plane *I*; *γ*: angle Cg(*I*) → Cg(*J*) vector and normal to plane *J*; slippage: distance between Cg(*I*) and perpendicular projection of Cg(*J*) on ring *I*. [b] Symmetry transformations used to generate equivalent atoms: #1 1 + *x*, *y*, *z*; #2 −1 + *x*, *y*, *z*. Cg(1): N(1A)–C(2A)–C(3A)–C(4A)–C(5A)–C(6A), Cg(2): N(12A)–C(11A)–C(16A)–C(15A)–C(14A)–C(13A). [c] Symmetry transformations used to generate equivalent atoms: #1 1 − *x*, 1 − *y*, 1 − *z*. Cg(4): N(1A)–C(2A)–C(3A)–C(4A)–C(5A)–C(6A); Cg(4): N(12A)–C(11A)–C(16A)–C(15A)–C(14A)–C(13A). [d] Symmetry transformations used to generate equivalent atoms: #1 1 − *x*, 1 − *y*, 1 − *z*. Cg(1): N(1A)–C(2A)–C(3A)–C(4A)–C(5A)–C(6A); Cg(2): N(12A)–C(11A)–C(16A)–C(15A)–C(14A)–C(13A). [e] Symmetry transformations used to generate equivalent atoms: #1 1 − *x*, 2 − *y*, 1 − *z*. Cg(4): N(1A)–C(2A)–C(3A)–C(4A)–C(5A)–C(6A). [f] Symmetry transformations used to generate equivalent atoms: #1 *x*, −1 + *y*, *z*; #2 1 + *x*, −1 + *y*, *z*; #3 −1 + *x*, 1 + *y*, *z*; #4 *x*, 1 + *y*, *z*. Cg(4): N(1A)–C(2A)–C(3A)–C(4A)–C(5A)–C(6A), Cg(5): N(12A)–C(11A)–C(16A)–C(15A)–C(14A)–C(13A). [g] Symmetry transformations used to generate equivalent atoms: #1 1/2 − *x*, −1/2 + *y*, 1/2 − *z*; #2 1 − *x*, −*y*, 1 − *z*; #3 1/2 − *x*, 1/2 + *y*, 1/2 − *z*. Cg(1): N(1A)–C(2A)–C(3A)–C(4A)–C(5A)–C(6A), Cg(2): N(12A)–C(11A)–C(16A)–C(15A)–C(14A)–C(13A). [h] Symmetry transformations used to generate equivalent atoms: #1 −*x*, 1 − *y*, 1 − *z*. Cg(1): N(1A)–C(2A)–C(3A)–C(4A)–C(5A)–C(6A), Cg(2): N(12A)–C(11A)–C(16A)–C(15A)–C(14A)–C(13A).

structure of $[H_2L]ClO_4$ is further stabilized by π···π stacking interactions (Table 2), formed between the polytypic aromatic rings of neighbouring ligand cations.

Single-crystal X-ray diffraction studies showed that in all the six complexes the Pb^{II} ion exhibits a hemidirected coordination geometry, and the metal ion participates in tetrel bonding (Table 3).

The asymmetric unit of $\{[PbL]ClO_4\}_n \cdot nH_2O$ contains one $[PbL]^+$ cation, in which the deprotonated parent ligand **L** is κ^3-coordinated, one ClO_4^- anion, with three oxygen atoms being disordered over two positions with a 58% and 42% ratio, and one molecule of water, disordered over three positions with a 40%, 30% and 30% ratio. The Pb^{II} atom is covalently linked (*d*[Pb–N/O] = 2.382(4)–2.513(4) Å) to two nitrogens and one oxygen atom of **L** and one 3-pyridyl nitrogen atom of another ligand **L** with the formation of a 1D zig-zag-like polymeric polycation (Fig. 2 and Table 3). All the covalent bonds are concentrated on one quarter of the globe of the coordination sphere with the closest approach of two atoms on the other side of about 230°. This leaves a large gap on the Pb^{II} ion, which enables a close approach of the non-disordered ClO_4^- oxygen atom (*d*[Pb···O] = 3.201(5) Å) and, remarkably, the amide nitrogen atom (*d*[Pb···N] = 2.934(4) Å) from the ligand **L** of an adjacent polymeric polycation (Fig. 2 and Table 3). The latter contacts interconnect the polymeric polycations into 2D sheets, which are further stabilized by π···π stacking interactions (Table 2), formed between the polytypic aromatic rings of neighbouring ligands **L**. These 2D sheets are separated by layers of ClO_4^- anions and H_2O molecules. Taking all the covalent and tetrel bonds into account, the coordination environment around the Pb^{II} cation in the structure of $\{[PbL]ClO_4\}_n \cdot nH_2O$ is best described as a distorted octahedron.

The asymmetric unit of $\{[Pb(HL)(OAc)]ClO_4\}_n$ contains one $[Pb(HL)(OAc)]^+$ cation, in which the neutral form of the parent ligand **HL** is κ^3-coordinated and the OAc^- anion is κ^2-coordinated to the same metal center, and one ClO_4^- anion. The Pb^{II} atom is covalently linked (*d*[Pb–N/O] = 2.372(5)–2.755(7) Å) to two nitrogens and one oxygen atom of **HL**, one 3-pyridyl nitrogen atom of another ligand **HL**, with the formation of a 1D zig-zag-like polymeric polycation (Fig. 3 and Table 3) similar to that in the structure of $\{[PbL]ClO_4\}_n \cdot nH_2O$ (Fig. 2), and two OAc^- oxygen atoms. All the covalent bonds are concentrated on one hemisphere of the coordination sphere with the closest approach of two atoms on the other side of about 205°. This also leaves a large gap on the Pb^{II} ion, which enables a close approach of the two ClO_4^- oxygen atoms (*d*[Pb···O] = 3.047(7) and 3.309(10) Å) (Fig. 3 and Table 3). The polymeric polycations are interconnected into 2D sheets through intermolecular N–H···O hydrogen bonds (Table 1), formed between the amide NH hydrogen atom of one cation and one of the OAc^- oxygen atoms of an adjacent cation, which are further stabilized by π···π stacking interactions (Table 2), formed between the polytypic aromatic rings of the same species. These 2D sheets are also separated by layers of ClO_4^- anions.

Table 3 Covalent and tetrel bond lengths (Å) in the structures of Pb^{II} complexes described in this work

Complex	Bond	Ligand	Length	Bond type
$\{[PbL]ClO_4\}_n \cdot nH_2O$	Pb–N	L	2.408(4)	Covalent
		L	2.507(4)	Covalent
		L	2.513(4)	Covalent
		L	2.934(4)	Tetrel
	Pb–O	L	2.382(4)	Covalent
		ClO_4^-	3.201(5)	Tetrel
$\{[Pb(HL)(OAc)]ClO_4\}_n$	Pb–N	L	2.612(6)	Covalent
		L	2.633(6)	Covalent
		L	2.755(7)	Covalent
	Pb–O	L	2.572(5)	Covalent
		OAc^-	2.372(5)	Covalent
		OAc^-	2.515(6)	Covalent
		ClO_4^-	3.047(7)	Tetrel
		ClO_4^-	3.309(10)	Tetrel
$[PbL(NO_2)]_n$	Pb–N	L	2.452(4)	Covalent
		L	2.535(5)	Covalent
		L	2.752(5)	Covalent
		L	3.258(4)	Tetrel
	Pb–O	L	2.384(5)	Covalent
		NO_2^-	2.547(4)	Covalent
		NO_2^-	2.904(5)	Covalent
		NO_2^-	3.299(4)	Tetrel
$[PbLN_3]_n$	Pb–N	L	2.571(3)	Covalent
		L	2.740(3)	Covalent
		L	2.837(3)	Covalent
		L	3.436(4)	Tetrel
		N_3^-	2.321(3)	Covalent
		N_3^-	2.883(3)	Covalent
	Pb–O	L	2.335(3)	Covalent
$[Pb_2(HL)_2(NO_3)_2(NCS)_2]$	Pb–N	L	2.663(3)	Covalent
		L	2.677(3)	Covalent
		L	2.809(3)	Covalent
		NCS^-	2.460(4)	Covalent
	Pb–O	L	2.555(2)	Covalent
		NO_3^-	2.744(2)	Covalent
		NO_3^-	2.882(2)	Covalent
	Pb–S	NCS^-	3.2246(11)	Tetrel
$[PbL(OAc)]_2$	Pb–N	L	2.490(3)	Covalent
		L	2.613(4)	Covalent
		L	3.030(4)	Tetrel
		L	3.409(4)	Tetrel
		L	3.489(3)	Tetrel
	Pb–O	L	2.383(3)	Covalent
		OAc^-	2.294(3)	Covalent
		OAc^-	2.753(4)	Covalent

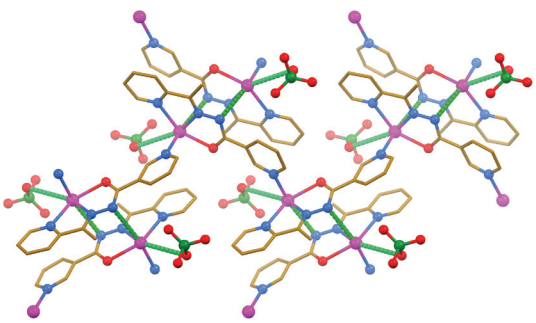

Fig. 2 Crystal structure of $\{[PbL]ClO_4\}_n \cdot nH_2O$ (hydrogen atoms and water molecules are omitted for clarity). Tetrel bonds Pb···N and Pb···O are shown as dashed lines. Stronger non-covalent interactions are shown in a darker shade of green than the weaker non-covalent interactions. Color code: C = gold, N = blue, Cl = green, O = red, Pb = magenta.

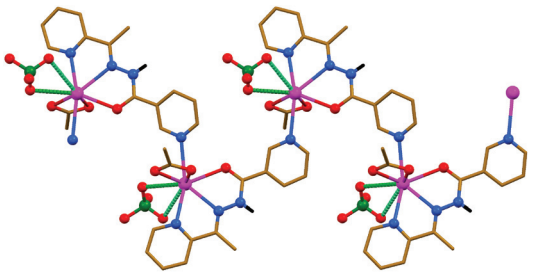

Fig. 3 Crystal structure of $\{[Pb(HL)(OAc)]ClO_4\}_n$ (CH hydrogen atoms are omitted for clarity). Tetrel bonds Pb···O are shown as dashed lines. Stronger non-covalent interactions are shown in a darker shade of green than the weaker non-covalent interactions. Color code: C = gold, H = black, N = blue, Cl = green, O = red, Pb = magenta.

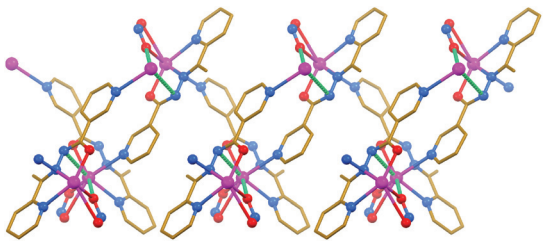

Fig. 4 Crystal structure of $[PbL(NO_2)]_n$ (hydrogen atoms are omitted for clarity). Tetrel bonds Pb···N and Pb···O are shown as dashed lines. Stronger non-covalent interactions are shown in a darker shade of green than the weaker non-covalent interactions. Color code: C = gold, N = blue, O = red, Pb = magenta.

The structure of $[PbL(NO_2)]_n$ is similar to that of $\{[PbL]ClO_4\}_n \cdot nH_2O$. The main difference, influencing the overall 1D zig-zag-like polymeric structure of the former complex (Fig. 4), however, arises from the NO_2^- anion, which is fully ordered and covalently bound to the metal center, yielding the $[PbL(NO_2)]$-containing asymmetric unit. The deprotonated form of the κ^3-coordinated parent ligand **L** and the κ^2-coordinated NO_2^- anion as well as the 3-pyridyl nitrogen atom of an adjacent ligand **L**, all being linked to the same metal cation, provides six covalent bonds (d[Pb–N/O] = 2.384(5)–2.904(5) Å) (Table 3). These bonds are concentrated on one hemisphere of the coordination sphere with the closest approach of two atoms on the other side of about 154°. This gap on the Pb^{II} ion enables a close approach of the amide nitrogen atom (d[Pb···N] = 3.258(4) Å) and one of the NO_2^- oxygen atoms (d[Pb···O] = 3.299(4) Å), arising from the same $[PbL(NO_2)]$ fragment of an adjacent polymeric chain (Fig. 4). The 1D polymeric chains are further interlinked through π···π stacking interactions (Table 2), formed between the 3-pyridyl rings, yielding 2D sheets.

The structures of $[PbLN_3]_n$, $[Pb_2(HL)_2(NO_3)_2(NCS)_2]$ and $[PbL(OAc)]_2$ are constructed from similar secondary building units (SBUs), each of which represent a dimeric aggregate with covalently κ^3-coordinated organic ligands (Fig. 5–7 and Table 3). This dimer is, however, of the $[Pb_2L_2]^{2+}$ structure in

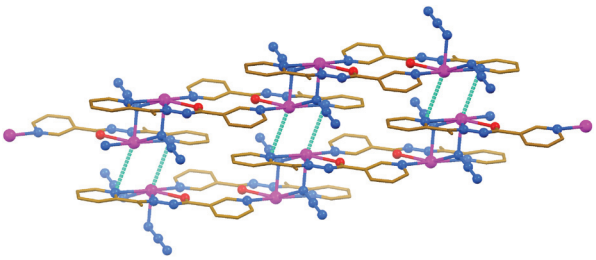

Fig. 5 Crystal structure of $[PbLN_3]_n$ (hydrogen atoms are omitted for clarity). Tetrel bonds Pb···N are shown as dashed lines. Color code: C = gold, N = blue, O = red, Pb = magenta.

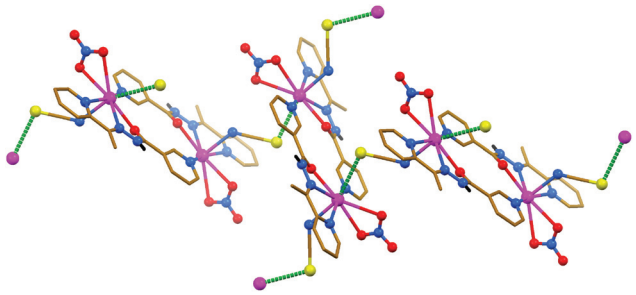

Fig. 6 Crystal structure of $[Pb_2(HL)_2(NO_3)_2(NCS)_2]$ (CH hydrogen atoms are omitted for clarity). Tetrel bonds Pb···S are shown as dashed lines. Color code: C = gold, H = black, N = blue, O = red, Pb = magenta, S = yellow.

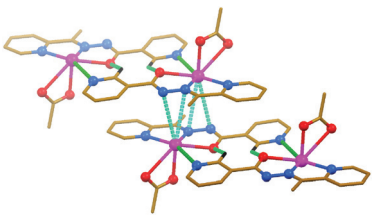

Fig. 7 Crystal structure of $[PbL(OAc)]_2$ (hydrogen atoms not-involved in H-bonding are omitted for clarity). Tetrel bonds Pb···N and hydrogen bonds are shown as dashed lines. Stronger non-covalent interactions are shown in a darker shade of green than the weaker non-covalent interactions. Color code: C = gold, H = black, N = blue, O = red, Pb = magenta.

the N_3^-- and OAc^--containing complexes, and of the $[Pb_2(HL)_2]^{4+}$ structure in the NCS^--containing compound. The asymmetric unit of $[PbLN_3]_n$ and $[PbL(OAc)]_2$ comprises [PbLX] (X = N_3^- or OAc^-, respectively) species, while [Pb(HL)(NO_3)(NCS)] was found in the asymmetric unit of $[Pb_2(HL)_2(NO_3)_2(NCS)_2]$. Notably, these mononuclear species in the structures of $[PbLN_3]_n$ and $[Pb_2(HL)_2(NO_3)_2(NCS)_2]$ are combined in SBUs through the Pb–N (2.837(3) and 2.809(3) Å, respectively) covalent bonds between the metal center of one monomeric species and the 3-pyridyl nitrogen atom of the other monomeric species (Fig. 5 and 6). The same aggregation in the structure of $[PbL(OAc)]_2$ is, however, due to the Pb···N (3.030(4) Å) tetrel bonding, and is further stabilized by the C–H···O hydrogen bonds (Fig. 7).

In the structure of $[PbLN_3]_n$, dimeric SBUs are linked in 1D ladder-like polymeric chains through the μ-1,1 (end-on) covalently coordinated N_3^- anions (Fig. 5 and Table 3). These 1D chains are interlinked through the Pb···N tetrel (3.436(4) Å) bonds, formed between the metal centers of the chain and the 2-pyridyl nitrogen atoms of an adjacent chain (Fig. 5). These interactions are also realized due to the concentration of the covalent bonds on one hemisphere of the coordination sphere with the closest approach of two atoms on the other side of about 197°. The 1D polymeric chains are further interlinked through π···π stacking interactions (Table 2), formed between the polytypic aromatic rings of neighbouring ligand cations.

In the structures of $[Pb_2(HL)_2(NO_3)_2(NCS)_2]$ and $[PbL(OAc)]_2$, the inorganic anions NO_3^- and OAc^-, respectively, are each covalently κ^2-coordinated to the metal center through two oxygen atoms, and the coordination sphere of the Pb^{II} ion in the former complex is further filled by the covalently bound nitrogen atom of the terminally coordinated NCS^- anion (Fig. 6 and 7 and Table 3). SBUs in the structure of $[Pb_2(HL)_2(NO_3)_2(NCS)_2]$ are linked into 2D sheets through the Pb···S tetrel (3.2246(11) Å) bonds, formed between the metal centers of the SBU and the NCS^- sulfur atoms of adjacent SBUs (Fig. 6). Such kind of tetrel bonding is not only due to the free sulfur donor atom of the terminally coordinated NCS^- anions but also due to a relatively small gap around the Pb^{II} ions (~151°). Tetrel bonded 2D sheets in the structure of $[Pb_2(HL)_2(NO_3)_2(NCS)_2]$ are linked into a 3D framework through the intermolecular N–H···O hydrogen bonds (Table 1), formed between the amide NH hydrogen atom of one SBU and one of the coordinated NO_3^- oxygen atoms of an adjacent SBU. This 3D framework is further stabilized by π···π stacking interactions (Table 2), formed between the polytypic aromatic rings of different SBUs. A significantly larger gap around the Pb^{II} ion (~232°) in the structure of $[PbL(OAc)]_2$ is responsible for the formation of Pb···N tetrel (3.409(4) and 3.489(3) Å) bonds with both hydrazide nitrogen atoms of an adjacent SBU (Fig. 7 and Table 3). As a result of tetrel bonding between SBUs, 2D sheets are formed in the structure of $[PbL(OAc)]_2$. These 2D sheets are additionally stabilized by π···π stacking interactions (Table 2), formed between the polytypic aromatic rings of different SBUs.

In order to rationalize the formation of various architectures of the synthesized compounds as well as to describe intermolecular interactions we have performed theoretical studies at the DFT/BLYP-D3/TZP level of theory as implemented in the Amsterdam Density Functional (ADF) package.[72,73] The relativistic effects are accounted by the ZORA approximation as implemented in the ADF program. We have discussed predominantly the DFT/BLYP-D3/TZP results because it has been shown that it provides satisfactory results for noncovalent interactions as compared with the accurate CCSD(T) results.[74–76] At the first stage we briefly analyze molecular electrostatic potentials (MEP) as they have been shown to provide very useful quantity to rationalize chemical structures

and reactivity[29–32] followed by in depth characterization of bonding patterns by means of the charge and energy decomposition scheme ETS-NOCV[77–79] as implemented in the ADF program. It must be emphasized that qualitative and quantitative descriptions of various non-covalent interactions in the Pb^{II} complexes with the nicotinohydrazine, based on the ETS-NOCV energy decomposition scheme, will be provided for the first time.

It was established that, although the Pb–**L** bond is formed due to a charge donation **L** → Pb^{II}, a significant electrophilic region (blue color) around the metal center is noticed (Fig. 8), which, in turn, promotes binding of anions. Further binding of an anion (*e.g.* OAc^-) decreases a positive charge at the Pb^{II} atom, resulting in less positive MEP values. However, still a large positive MEP area is noted around the metal (Fig. S1 in the ESI†). This explains that the entire Pb^{II} sphere participates in various binding modes in the synthesized compounds.

We have further performed an in depth bonding analysis on the example of **[PbL(OAc)]$_2$** by means of the ETS-NOCV

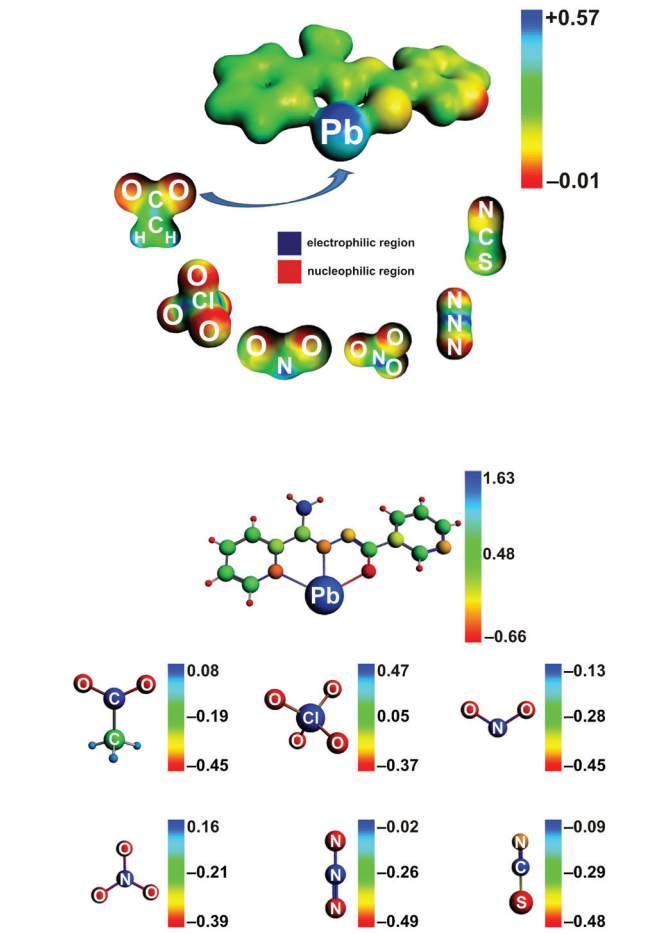

Fig. 8 (Top) Molecular electrostatic potentials (DFT/BLYP-D3/ZORA/TZP), describing the $[PbL]^+$ unit and anions (OAc^-, ClO_4^-, NO_2^-, NO_3^-, N_3^- and NCS^-). (Bottom) The Hirshfeld atomic charges of the $[PbL]^+$ unit and anions (OAc^-, ClO_4^-, NO_2^-, NO_3^-, N_3^- and NCS^-). In order to differentiate the charge distribution at various regions of the selected ions, the optimal electron density contour value was chosen as 0.03 a. u.

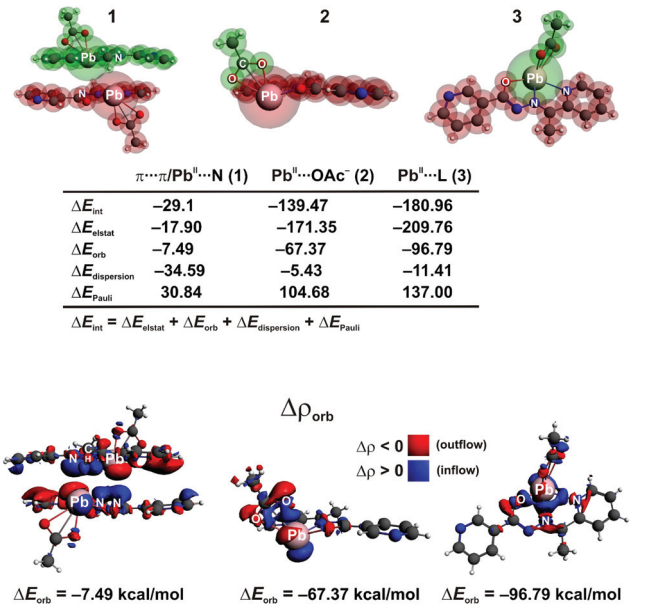

	π···π/Pb^{II}···N (1)	Pb^{II}···OAc$^-$ (2)	Pb^{II}···L (3)
ΔE_{int}	−29.1	−139.47	−180.96
ΔE_{elstat}	−17.90	−171.35	−209.76
ΔE_{orb}	−7.49	−67.37	−96.79
$\Delta E_{dispersion}$	−34.59	−5.43	−11.41
ΔE_{Pauli}	30.84	104.68	137.00

$\Delta E_{int} = \Delta E_{elstat} + \Delta E_{orb} + \Delta E_{dispersion} + \Delta E_{Pauli}$

Fig. 9 (Top) Cluster models of **[PbL(OAc)]$_2$** together with the fragmentation patterns **1–3** applied in the ETS-NOCV analysis. (Bottom) The overall deformation densities $\Delta\rho_{orb}$ of **1–3** with the corresponding energies ΔE_{orb}.

method, using the cluster models (Fig. 9). This allowed us to shed light on various bonding modes, labeled as **1–3** in Fig. 9, that stabilize **[PbL(OAc)]$_2$**. Polytypic rings of the two parallel oriented units [Pb**L**(OAc)] give rise to the π···π interaction energy ΔE_{int} = −29.14 kcal mol^{-1}. The main stabilizing factor appeared to be the dispersion ($\Delta E_{dispersion}$ = −34.59 kcal mol^{-1}) followed by the electrostatic (ΔE_{elstat} = −17.9 kcal mol^{-1}) and charge transfer/polarization (ΔE_{orb} = −7.49 kcal mol^{-1}) contributions (Fig. 9). It is important to note that the presence of heteroatoms in the $[PbL]^+$ species enforces additionally the formation of the Pb···N tetrel bonding, as evidenced from the contour of the overall deformation density $\Delta\rho_{orb}$. In particular, both the charge donation from the Pb^{II} atom (6s electrons) to the empty π*(N=N) as well as back-donation from the occupied π(N=N) to the metal center are noted (Fig. 9). Therefore, the Pb^{II} atom acts here as both the electron donor and acceptor. Hence, the red and blue colors of $\Delta\rho_{orb}$ are visible on Pb^{II}. A closer inspection of $\Delta\rho_{orb}$ reveals a charge transfer from the methyl σ(C–H) bonds of **L** onto the Pb^{II}, which demonstrates the formation of the agostic interaction Pb···CH. The π···π stacking, Pb···N and Pb···CH interactions are all together present in this system. It is to be referenced that such interactions have been also found in other Pb^{II} compounds.[63–66,80–83] Considering the remaining bonds Pb–OAc^- and Pb–**L** (**2** and **3**, respectively, in Fig. 9), far lower interaction energies (ΔE_{int} = −139.47 and −180.96 kcal mol^{-1}, respectively) are noticed. They are dominated by the electrostatic factor followed by the orbital and dispersion terms (Fig. 9). As far as changes in the electron density are concerned ($\Delta\rho_{orb}$), the Pb–OAc^- and Pb–L bonds are due to the donation

(AcO^-/**L** → Pb^{II}) and back-donation (Pb^{II} → AcO^-/**L**) channels (Fig. 9). Notably, although the interaction energies change significantly when comparing **1–3**, the overall picture, emerging from the deformation density ($\Delta\rho_{orb}$), remains essentially very similar. In particular, all bonding types result from the donor–acceptor (dative) interactions giving rise additionally to the charge accumulation in the binding region (covalent contribution). Accordingly, these interactions, including the tetrel one, fall within the group of dative-covalent connections. It should be added that **2** and **3** are evidently more covalent as compared with **1** as it can be deduced from the contours of $\Delta\rho_{orb}$ (Fig. 9).

We have also performed the charge and energy decomposition calculations for various cluster models of the remaining compounds and the obtained results are shown in Fig. S2–S6 in the ESI.† For the sake of brevity, we will not discuss in detail each type of the bonding pattern and only the most relevant and interesting observations will be highlighted below.

The [Pb**L**$(NO)_2$] units in the structure of **[PbL(NO$_2$)]$_n$** are quasi-perpendicular (Fig. 4). This leads to the formation of "pure" tetrel bonding Pb···N (labelled as **1** in Fig. S2 in the ESI†). This strong interaction (ΔE_{int} = −20.55 kcal mol^{-1}) is from two equally important stabilizing factors, namely the dispersion ($\Delta E_{dispersion}$ = −19.83 kcal mol^{-1}) and electrostatic (ΔE_{elstat} = −18.38 kcal mol^{-1}) factors (Fig. S2 in the ESI†). The overall deformation density $\Delta\rho_{orb}$ demonstrates that the Pb···N interaction leads, similarly to **[PbL(OAc)]$_2$**, to donor–acceptor electron density delocalizations Pb^{II} → π*(N=N) and π(N=N) → Pb^{II} (Fig. S2 in the ESI†). Similar to the Pb–OAc^- and Pb–L bonds, the Pb–NO_2^- connection (labeled as **2** in Fig. S2 in the ESI†) is electrostatically dominated and it contains the dative-covalent contributions.

In the case of the **[PbLN$_3$]$_n$** structure, the [Pb**L**N_3] units are also aligned. However, the bonding pattern (labelled as **1** in Fig. S3 in the ESI†), emerging from the deformation density $\Delta\rho_{orb}$, is quite distinctive as compared with the remaining structures (Fig. S3 in the ESI†). Surprisingly, not only the charge accumulation (blue color of $\Delta\rho_{orb}$) in the Pb···N region is observed, but predominantly between the Pb^{II} centers (Fig. S3 in the ESI†). The latter is entirely non-intuitive because of the electrophilic nature of the lead centers. It is more clearly visible when considering the specific NOCV-based deformation density contributions $\Delta\rho_1(1)$ + $\Delta\rho_2(2)$, corresponding to $\Delta E_{orb}(1)$ + $\Delta E_{orb}(2)$ = −2.0 kcal mol^{-1}, which clearly depicts the Pb^{II}···Pb^{II} interaction, and $\Delta\rho_3(3)$, displaying the formation of the tetrel-bonding Pb···N as a part of the π···π stacking interaction (Fig. S3 in the ESI†). It could be anticipated, based on the above findings, that novel supramolecular architectures induced by non-covalent Pb^{II}···Pb^{II} interactions are expected to be prepared in the future.

It should be noted that the existence of weak and rare Pb^{II}···Pb^{II} bonding has also been suggested by Caruso and co-workers in the polymeric bis(pyrrolidinecarbodithioato)lead(II),[84] and by Power *et al.* in Pb(C_6H_4-4-But)ArPr_2.[85] More recently, the Au^{I}···Pb^{II} interaction has been determined in the structure of [Pb{HB(pz)$_3$}Au(C_6Cl_5)$_2$].[86]

The model **2** is suitable for the description of "pure" tetrel bonding Pb···N in **[PbLN$_3$]$_n$** (Fig. S3 in the ESI†). The results depicted as the second entry of the table demonstrate that the tetrel bonding in **[PbLN$_3$]$_n$** is predominantly electrostatic in nature (ΔE_{elstat} = −35.57 kcal mol^{-1}) followed by the orbital (ΔE_{orb} = −14.66 kcal mol^{-1}) and dispersion ($\Delta E_{dispersion}$ = −10.76 kcal mol^{-1}) contributions. It should be noted that the electrostatic and dispersion terms are equally important in the case of **[PbL(NO$_2$)]$_n$** (Fig. S2 in the ESI†). This clearly demonstrates that the same type of bonding may be constituted from quantitatively different forces in various crystal motifs.

As far as binding of anions is concerned, the results of ETS-NOCV calculations allowed us to observe that each bond Pb–X (X = NO_3^-, ClO_4^-, N_3^-, NCS^- and OAc^-) can generally be ascribed as dative-covalent (donor–acceptor) as it can be inferred from the change in the electron density ($\Delta\rho_{orb}$) due to the formation of Pb–X bonds (Fig. 9 and Fig. S2–S6 in the ESI†). Furthermore, they are dominated by the electrostatic contribution followed by the orbital interaction and dispersion components. As far as the strength of the interaction is concerned one can summarize that the obtained interaction energies cover a wide range starting from very weak for X = **L**, ΔE_{int} = −6.15 kcal mol^{-1} (Fig. S6 in the ESI†) in **{[PbL]ClO$_4$}$_n$·nH$_2$O** through ΔE_{int} = −74.53 kcal mol^{-1} for X = ClO_4^- in **{[Pb(HL)(OAc)]ClO$_4$}$_n$** (Fig. S4 in the ESI†) and ending up with the strongest one ΔE_{int} = −180.96 kcal mol^{-1} for X = L in **[PbL(OAc)]$_2$** (Fig. 9). Similarly, the ClO_4^- anions in **[H$_2$L]ClO$_4$** appeared to strongly interact with the cations $[H_2L]^+$ (ΔE_{int} = −67.4 or −69.43 kcal mol^{-1} depending on the cluster model) predominantly through the electrostatic forces. These contributions constitute predominantly the ClO_4^-···π and NH···O interactions (Fig. S7 in the ESI†).

Conclusions

In summary, we have designed six new Pb^{II} complexes with the *N*′-(1-(2-pyridyl)ethylidene)nicotinohydrazide (**HL**) ligand. The nature of the inorganic anion is also important for the final structure. In all the complexes the Pb^{II} center exhibits a hemidirected coordination geometry with all the covalent bonds being concentrated on one hemisphere of the coordination sphere with the closest approach of two atoms on the other side varying from 151° to 232°. The sterically available Pb^{II} ion participates in tetrel bonding, as evidenced from the detailed structural analysis of the described complexes. These tetrel bonds play a key role in the supramolecular aggregation of building units of all the structures in the solid state. As a result of tetrel bonding, the structures of all the six compounds can be extended to a higher dimensional framework, which is further stabilized by π···π stacking interactions between the aromatic rings. The charge and energy decomposition calculations (ETS-NOCV) allowed us to identify and quantify the nature of non-covalent interactions that stabilize the obtained structures. Importantly, apart from the mentioned non-covalent interactions (π···π stacking and tetrel

bonds), the ETS-NOCV method allowed us to identify and quantify for the first time a rare example of $Pb^{II}\cdots Pb^{II}$ interactions. It allows one to envisage that novel supramolecular architectures, driven by non-covalent $Pb^{II}\cdots Pb^{II}$ interactions, might be prepared in the close future. Finally, it has been determined that the anions bind to Pb^{II} predominantly through the electrostatic forces, however, the dative-covalent contributions also appeared to be important.

Experimental

Materials

The Schiff base **HL** was prepared by following the reported method as described elsewhere[69] and used without further purification. All other reagents and solvents used for synthesis and analysis were commercially available and used as received.

Physical measurements

FTIR spectra were recorded on a Bruker Tensor 27 FTIR spectrometer. Microanalyses were performed with a Heraeus CHN-O-Rapid analyzer.

DFT calculations

We have performed the DFT calculations based on the BLYP-D3/ZORA/TZP level as implemented in the ADF suit of programs.[72,73] The charge and energy decomposition scheme ETS-NOCV[77–79] has been applied in order to characterize the stability of the obtained structures.

ETS-NOCV bonding analysis

The natural orbitals for chemical valence (NOCV)[77–79] are eigenvectors that diagonalize the deformation density matrix:

$$\Delta PC_i = \nu_i C_i \quad \Psi_i = \sum_j^N C_{i,j}\lambda_j,$$

where C_i is a vector of coefficients, expanding Ψ_i in the basis of fragment orbitals λ_j; N is a total number of fragment λ_j orbitals. It was shown that the natural orbitals for chemical valence pairs (ψ_{-k},ψ_k) decompose the differential density $\Delta\rho$ into NOCV-contributions $(\Delta\rho_k)$:

$$\Delta\rho(r) = \sum_{k=1}^{M/2}\nu_k[-\psi_{-k}{}^2(r) + \psi_k{}^2(r)] = \sum_{k=1}^{M/2}\Delta\rho_k(r),$$

where ν_k and M stand for the NOCV eigenvalues and the number of basis functions, respectively. Visual inspection of deformation density plots $(\Delta\rho_k)$ helps to attribute symmetry and the direction of the charge flow. In addition, these pictures are enriched by providing the energetic estimations, $\Delta E_{orb}(k)$, for each $\Delta\rho_k$ within the ETS-NOCV scheme.[76–78] The exact formula, which links the ETS and NOCV methods, will be given in the next paragraph, after we briefly present the basic concept of the ETS scheme. In this method the total bonding energy, ΔE_{int}, between interacting fragments, exhibiting the geometry as in the combined complex, is divided into three components: $\Delta E_{total} = \Delta E_{elstat} + \Delta E_{Pauli} + \Delta E_{orb}$. The first term, ΔE_{elstat}, corresponds to the classical electrostatic interaction between the promoted fragments as they are brought to their positions in the final complex. The second term, ΔE_{Pauli}, accounts for the repulsive Pauli interaction between occupied orbitals on the two fragments in the combined molecule. Finally, the last stabilizing term, ΔE_{orb}, represents interactions between the occupied molecular orbitals of one fragment with the unoccupied molecular orbitals of the other fragment as well as mixing of occupied and virtual orbitals within the same fragment (inner-fragment polarization). This energy term may be linked to the electronic bonding effect coming from the formation of a chemical bond. In the combined ETS-NOCV scheme the orbital interaction term (ΔE_{orb}) is expressed in terms of NOCV's eigenvalues (ν_k) as:

$$\Delta E_{orb} = \sum_k \Delta E_{orb}(k) = \sum_{k=1}^{M/2}\nu_k[-F^{TS}_{-k,-k} + F^{TS}_{k,k}],$$

where $F_{i,i}{}^{TS}$ are diagonal Kohn–Sham matrix elements defined over NOCV with respect to the transition state (TS) density at the midpoint between density of the molecule and the sum of fragment densities. The above components $\Delta E_{orb}(k)$ provide the energetic estimation of $\Delta\rho_k$ that may be related to the importance of a particular electron flow channel for the bonding between the considered molecular fragments. The ETS-NOCV analysis was done based on the Amsterdam Density Functional (ADF) package[72,73] in which this scheme was implemented.

Synthesis of $\{[PbL]ClO_4\}_n\cdot nH_2O$

HL (0.024 g, 0.1 mmol) and $Pb(ClO_4)_2$ (0.041 g, 0.1 mmol) were placed in the main arm of a branched tube. MeOH (15 mL) was carefully added to fill the arms. The tube was sealed and immersed in an oil bath at 60 °C while the branched arm was kept at ambient temperature. X-ray suitable yellow prism-like crystals were formed during the next days in the cooler arm and were filtered off, washed with acetone and diethyl ether, and dried in air. Yield: 0.049 g (86.9%). FTIR, ν: 624, 910 and 1078 (ClO_4^-), 1638 and 3452 (H_2O), 1590 (C=O) cm^{-1}. Anal. Calc. for $C_{13}H_{13}ClN_4O_6Pb$ (563.92) (%): C 27.69, H 2.32 and N 9.94; found: C 28.1, H 2.2 and N 10.2.

Synthesis of $\{[Pb(HL)(OAc)]ClO_4\}_n$ and $[PbL(NO_2)]_n$

HL (0.024 g, 0.1 mmol), $Pb(ClO_4)_2$ (0.041 g, 0.1 mmol) and NaOAc or $NaNO_2$ (0.016 and 0.014 g, respectively; 0.2 mmol) were placed in the main arm of a branched tube. MeOH (15 mL) was carefully added to fill the arms. The tube was sealed and immersed in an oil bath at 60 °C while the branched arm was kept at ambient temperature. X-ray suitable crystals were formed during the next days in the cooler arm and were filtered off, washed with acetone and diethyl ether, and dried in air.

$\{[Pb(HL)(OAc)]ClO_4\}_n$. Green plate-like crystals. Yield: 0.046 g (75.8%). FTIR, ν: 683 and 1154 (ClO_4^-), 1468 and 1500 (OAc^-), 1572 (C=O), 3469 (NH) cm^{-1}. Anal. Calc. for

$C_{15}H_{15}ClN_4O_7Pb$ (605.96) (%): C 29.73, H 2.50 and N 9.25; found: C 30.1, H 2.6 and N 9.3.

$[PbL(NO_2)]_n$. Yellow plate-like crystals. Yield: 0.034 g (69.0%). FTIR, ν: 1162 and 1271 (NO_2^-), 1596 (C═O) cm^{-1}. Anal. Calc. for $C_{13}H_{11}N_5O_3Pb$ (492.46) (%): C 31.71, H 2.25 and N 14.22; found: C 31.5, H 2.4 and N 13.9.

Synthesis of $[H_2L]ClO_4$, $[PbLN_3]_n$ and $[Pb_2(HL)_2(NO_3)_2(NCS)_2]$

A solution of **HL** (0.024 g, 0.1 mmol) in MeOH (10 ml) was added dropwise to a solution of $Pb(NO_3)_2$ (0.033 g, 0.1 mmol) in the same solvent (10 ml). To this mixture, a solution of $NaClO_4$ or NaN_3 or NaNCS (0.024, 0.013 and 0.016 g, respectively; 0.2 mmol) in MeOH (5 ml) was added slowly under stirring. The resulting mixture was stirred at room temperature for 1 h and was left undisturbed for slow evaporation. X-ray suitable crystals were formed during the next days.

$[H_2L]ClO_4$. Colorless plate-like crystals. Yield: 0.016 g (47.0%). FTIR, ν: 621 and 1028 (ClO_4^-), 1698 (C═O), 3448 and 3747 (NH) cm^{-1}. Anal. Calc. for $C_{13}H_{13}ClN_4O_5$ (340.72) (%): C 45.83, H 3.85 and N 16.44; found: C 45.6, H 3.7 and N 16.2.

$[PbLN_3]_n$. Green-yellow plate-like crystals. Yield: 0.034 g (69.6%). FTIR, ν: 1579 (C═O), 1365 and 2035 (N_3^-) cm^{-1}. Anal. Calc. for $C_{13}H_{11}N_7OPb$ (488.48) (%): C 31.97, H 2.27 and N 20.07; found: C 32.0, H 2.4 and N 19.4.

$[Pb_2(HL)_2(NO_3)_2(NCS)_2]$. Green-yellow plate-like crystals. Yield: 0.031 g (54.6%). FTIR, ν: 1422 (NO_3^-), 1627 (C═O), 2030 (NCS^-), 3421 (NH) cm^{-1}. Anal. Calc. for $C_{28}H_{24}N_{12}O_8Pb_2S_2$ (1135.09) (%): C 29.63, H 2.13 and N 14.81; found: C 29.8, H 2.0 and N 14.5.

Synthesis of $[PbL(OAc)]_2$

A solution of **HL** (0.024 g, 0.1 mmol) in MeOH (10 ml) was added dropwise to a solution of $Pb(OAc)_2{\cdot}3H_2O$ (0.038 g, 0.1 mmol) in the same solvent (10 ml). The resulting mixture was stirred at room temperature for 1 h and left undisturbed for slow evaporation. X-ray suitable green plate-like crystals were formed during the next days. Yield: 0.040 g (79.1%). FTIR, ν: 1457 and 1507 (OAc^-), 1574 (C═O) cm^{-1}. Anal. Calc. for $C_{30}H_{28}N_8O_6Pb_2$ (1011.00) (%): C 35.64, H 2.79 and N 11.08; found: C 35.0, H 2.6 and N 11.4.

Single-crystal X-ray diffraction study

The X-ray data were collected on a Bruker four-circle single crystal diffractometer with a sealed graphite-monochromatised Mo-Kα (λ = 0.71073 Å) radiation tube and APEX-II CCD or SMART1000 CCD detectors. The structures were solved with SIR92 [87] and refined with the full-matrix least-squares procedure on $|F^2|$ by SHELXL-2013.[88] Non-hydrogen atoms were anisotropically refined and the hydrogen atoms were placed at calculated positions in riding mode with temperature factors fixed at 1.2 times U_{eq} of the parent atoms. Figures were generated using the program Mercury.[89]

Crystal data for $[H_2L]ClO_4$. $C_{13}H_{13}N_4O$, ClO_4; M_r = 340.72 g mol^{-1}, T = 100(1) K, monoclinic, space group $P2_1/c$, a = 8.151(3), b = 8.049(3), c = 21.772(9) Å, β = 94.501(6)°, V = 1424.0(10) $Å^3$, Z = 4, ρ = 1.589 g cm^{-3}, μ(Mo-Kα) = 0.302 mm^{-1}, reflections: 8470 collected, 2046 unique, R_{int} = 0.151, R_1(all) = 0.1672, wR_2(all) = 0.2144.

Crystal data for $\{[PbL]ClO_4\}_n{\cdot}nH_2O$. $C_{13}H_{11}N_4OPb$, ClO_4, O; M_r = 561.90 g mol^{-1}, T = 193(2) K, monoclinic, space group $P2_1/n$, a = 10.0724(8), b = 13.9283(11), c = 13.2362(10) Å, β = 112.065(1)°, V = 1720.9(2) $Å^3$, Z = 4, ρ = 2.169 g cm^{-3}, μ(Mo-Kα) = 9.996 mm^{-1}, reflections: 9073 collected, 3042 unique, R_{int} = 0.025, R_1(all) = 0.0274, wR_2(all) = 0.0718.

Crystal data for $\{[Pb(HL)(OAc)]ClO_4\}_n$. $C_{15}H_{15}N_4O_3Pb$, ClO_4; M_r = 605.95 g mol^{-1}, T = 296(2) K, orthorhombic, space group $Pbca$, a = 12.8619(4), b = 15.9903(5), c = 18.1591(6) Å, V = 3734.7(2) $Å^3$, Z = 8, ρ = 2.155 g cm^{-3}, μ(Mo-Kα) = 9.225 mm^{-1}, reflections: 14 736 collected, 3288 unique, R_{int} = 0.069, R_1(all) = 0.0604, wR_2(all) = 0.0936.

Crystal data for $[PbL(NO_2)]_n$. $C_{13}H_{11}N_5O_3Pb$, M_r = 492.46 g mol^{-1}, T = 193(2) K, monoclinic, space group $P2_1/c$, a = 15.4332(16), b = 9.372(1), c = 10.1192(10) Å, β = 102.149(2)°, V = 1430.9(3) $Å^3$, Z = 4, ρ = 2.286 g cm^{-3}, μ(Mo-Kα) = 11.812 mm^{-1}, reflections: 10 487 collected, 2521 unique, R_{int} = 0.044, R_1(all) = 0.0331, wR_2(all) = 0.0829.

Crystal data for $[PbLN_3]_n$. $C_{13}H_{11}N_7OPb$, M_r = 488.48 g mol^{-1}, T = 296(2) K, triclinic, space group $P\bar{1}$, a = 7.4765(3), b = 9.8748(5), c = 10.3866(9) Å, α = 85.982(6), β = 77.230(7), γ = 71.633(6)°, V = 709.77(8) $Å^3$, Z = 2, ρ = 2.286 g cm^{-3}, μ(Mo-Kα) = 11.899 mm^{-1}, reflections: 14 106 collected, 4097 unique, R_{int} = 0.038, R_1(all) = 0.0263, wR_2(all) = 0.0619.

Crystal data for $[Pb_2(HL)_2(NO_3)_2(NCS)_2]$. $C_{14}H_{12}N_6O_4PbS$, M_r = 567.56 g mol^{-1}, T = 296(2) K, monoclinic, space group $P2_1/n$, a = 9.6025(1), b = 14.5202(2), c = 12.4996(2) Å, β = 100.7659(7)°, V = 1712.15(4) $Å^3$, Z = 4, ρ = 2.202 g cm^{-3}, μ(Mo-Kα) = 10.010 mm^{-1}, reflections: 20 335 collected, 4989 unique, R_{int} = 0.036, R_1(all) = 0.0327, wR_2(all) = 0.0535.

Crystal data for $[PbL(OAc)]_2$. $C_{15}H_{14}N_4O_3Pb$, M_r = 505.49 g mol^{-1}, T = 296(2) K, monoclinic, space group $P2_1/c$, a = 8.7072(1), b = 20.7055(3), c = 8.9634(1) Å, β = 103.0686(6)°, V = 1574.13(3) $Å^3$, Z = 4, ρ = 2.133 g cm^{-3}, μ(Mo-Kα) = 10.738 mm^{-1}, reflections: 30 250 collected, 4587 unique, R_{int} = 0.044, R_1(all) = 0.0413, wR_2(all) = 0.0920.

Acknowledgements

We are grateful to the University of Maragheh for the financial support of this research. DFT calculations were partially performed using the PL-Grid Infrastructure and resources provided by the ACC Cyfronet AGH (Cracow, Poland).

References

1 J. An, S. J. Geib and N. L. Rosi, *J. Am. Chem. Soc.*, 2009, **131**, 8376.
2 M. C. Das and P. K. Bharadwaj, *J. Am. Chem. Soc.*, 2009, **131**, 10942.
3 R. Wang, J. Zhang and L. Li, *Inorg. Chem.*, 2009, **48**, 7194.

4 L. Ma, J. M. Falkowski, C. Abney and W. Lin, *Nat. Chem.*, 2010, **2**, 838.
5 H. L. Jiang, Y. Tatsu, Z. H. Lu and Q. Xu, *J. Am. Chem. Soc.*, 2010, **132**, 5586.
6 L. Duan, Z. H. Wu, J. P. Ma, X. W. Wu and Y. B. Dong, *Inorg. Chem.*, 2010, **49**, 11164.
7 P. Lama, A. Aijaz, E. C. Sañudo and P. K. Bharadwaj, *Cryst. Growth Des.*, 2010, **10**, 283.
8 G. C. Xu, W. Zhang, X. M. Ma, Y. H. Chen, L. Zhang, H. L. Cai, Z. M. Wang, R. G. Xiong and S. Gao, *J. Am. Chem. Soc.*, 2011, **133**, 14948.
9 M. K. Sharma, I. Senkovska, S. Kaskel and P. K. Bharadwaj, *Inorg. Chem.*, 2011, **50**, 539.
10 P. Pachfule, R. Das, P. Poddar and R. Banerjee, *Inorg. Chem.*, 2011, **50**, 3855.
11 M. P. Suh, H. J. Park, T. K. Prasad and D. W. Lim, *Chem. Rev.*, 2012, **112**, 782.
12 J. R. Li, J. Sculley and H. C. Zhou, *Chem. Rev.*, 2012, **112**, 869.
13 Y. Cui, Y. Yue, G. Qian and B. Chen, *Chem. Rev.*, 2012, **112**, 1126.
14 J. M. Roberts, B. M. Fini, A. A. Sarjeant, O. K. Farha, J. T. Hupp and K. A. Scheidt, *J. Am. Chem. Soc.*, 2012, **134**, 3334.
15 N. B. Shustova, A. F. Cozzolino and M. Dincă, *J. Am. Chem. Soc.*, 2012, **134**, 19596.
16 P. Kanoo, S. K. Reddy, G. Kumari, R. Haldar, C. Narayana, S. Balasubramanian and T. K. Maji, *Chem. Commun.*, 2012, **48**, 8487.
17 S. S. Nagarkar, A. K. Chaudhari and S. K. Ghosh, *Inorg. Chem.*, 2012, **51**, 572.
18 M. Ahmad, M. K. Sharma, R. Das, P. Poddar and P. K. Bharadwaj, *Cryst. Growth Des.*, 2012, **12**, 1571.
19 B. A. Blight, R. G. Nicolas, F. Kleitz, R. Y. Wang and S. Wang, *Inorg. Chem.*, 2013, **52**, 1673.
20 Y. Z. Tang, M. Zhou, J. Huang, Y. H. Tan, J. S. Wu and H. R. Wen, *Inorg. Chem.*, 2013, **52**, 1679.
21 A. Santra, I. Senkovska, S. Kaskel and P. K. Bharadwaj, *Inorg. Chem.*, 2013, **52**, 7358.
22 Z.-W. Wang, C.-C. Ji, J. Li, Z.-J. Guo, Y.-Z. Li and H.-G. Zheng, *Cryst. Growth Des.*, 2009, **9**, 475.
23 F. Luo, Y.-X. Che and J.-M. Zheng, *Cryst. Growth Des.*, 2009, **9**, 1066.
24 R. Sarma, D. Kalita and J. B. Baruah, *Dalton Trans.*, 2009, 7428.
25 D. Sun, H.-R. Xu, C.-F. Yang, Z.-H. Wei, N. Zhang, R.-B. Huang and L.-S. Zheng, *Cryst. Growth Des.*, 2010, **10**, 4642.
26 K.-L. Zhang, Y. Chang, C.-T. Hou, G.-W. Diao, R. Wu and S. W. Ng, *CrystEngComm*, 2010, **12**, 1194.
27 G. V. Oshovsky, D. N. Reinhoudt and W. Verboom, *Angew. Chem., Int. Ed.*, 2007, **46**, 2366.
28 J. M. Zayed, N. Nouvel, U. Rauwald and O. A. Scherman, *Chem. Soc. Rev.*, 2010, **39**, 2806.
29 J. S. Murray, P. Lane and P. Politzer, *J. Mol. Model.*, 2009, **15**, 723.
30 J. S. Murray, K. E. Riley, P. Politzer and T. Clark, *Aust. J. Chem.*, 2010, **63**, 1598.
31 P. Politzer, J. S. Murray and T. Clark, *Phys. Chem. Chem. Phys.*, 2013, **15**, 11178.
32 A. Bauzá, T. J. Mooibroek and A. Frontera, *ChemPhysChem*, 2015, **16**, 2496.
33 G. R. Desiraju and R. Parthasarathy, *J. Am. Chem. Soc.*, 1989, **111**, 8725.
34 P. Metrangolo and G. Resnati, *Chem. – Eur. J.*, 2001, **7**, 2511.
35 G. Cavallo, P. Metrangolo, T. Pilati, G. Resnati, M. Sansotera and G. Terraneo, *Chem. Soc. Rev.*, 2010, **39**, 3772.
36 P. Metrangolo and G. Resnati, *Halogen Bonding: Fundamentals and Applications (Stucture and Bonding)*, Springer, Heidelberg, 2010.
37 S. J. Grabowski, *Phys. Chem. Chem. Phys.*, 2013, **15**, 7249.
38 P. Metrangolo and G. Resnati, *Chem. Commun.*, 2013, **49**, 1783.
39 A. Mukherjee, S. Tothadi and G. R. Desiraju, *Acc. Chem. Res.*, 2014, **47**, 2514.
40 G. Cavallo, P. Metrangolo, R. Milani, T. Pilati, A. Priimagi, G. Resnati and G. Terraneo, *Chem. Rev.*, 2016, **116**, 2478.
41 H. Wang, W. Wang and W. J. Jin, *Chem. Rev.*, 2016, **116**, 5072.
42 M. Iwaoka, S. Takemoto and S. Tomoda, *J. Am. Chem. Soc.*, 2002, **124**, 10613.
43 C. Bleiholder, D. B. Werz, H. Köppel and R. Gleiter, *J. Am. Chem. Soc.*, 2006, **128**, 2666.
44 W. Z. Wang, B. M. Ji and Y. Zhang, *J. Phys. Chem. A*, 2009, **113**, 8132.
45 P. Metrangolo and G. Resnati, *Nat. Chem.*, 2012, **4**, 437.
46 M. Bai, S. P. Thomas, R. Kottokkaran, S. K. Nayak, P. C. Ramamurthy and T. N. G. Row, *Cryst. Growth Des.*, 2014, **14**, 459.
47 M. D. Esrafili, F. Mohammadian-Sabet and M. Solimannejad, *Struct. Chem.*, 2014, **25**, 1197.
48 U. Adhikari and S. Scheiner, *J. Phys. Chem. A*, 2014, **118**, 3183.
49 V. de P. N. Nziko and S. Scheiner, *J. Phys. Chem. A*, 2014, **118**, 10849.
50 L. M. Azofra, I. Alkorta and S. Scheiner, *J. Phys. Chem. A*, 2015, **119**, 535.
51 M. S. Balakrishna, D. J. Eisler and T. Chivers, *Chem. Soc. Rev.*, 2007, **36**, 650.
52 S. Zahn, R. Frank, E. Hey-Hawkins and B. Kirchner, *Chem. – Eur. J.*, 2011, **17**, 6034.
53 S. Scheiner, *Acc. Chem. Res.*, 2013, **46**, 280.
54 J. S. Murray, P. Lane and P. Politzer, *J. Mol. Model.*, 2009, **15**, 7239.
55 A. Bauzá, T. J. Mooibroek and A. Frontera, *Angew. Chem., Int. Ed.*, 2013, **52**, 12317.
56 A. Bundhun, P. Ramasami, J. S. Murray and P. Politzer, *J. Mol. Model.*, 2013, **19**, 2739.
57 A. Bauzá, T. J. Mooibroek and A. Frontera, *Chem. Commun.*, 2014, **50**, 12626.

58 A. Bauzá, T. J. Mooibroek and A. Frontera, *Chem. – Eur. J.*, 2014, **20**, 10245.
59 S. J. Grabowski, *Phys. Chem. Chem. Phys.*, 2014, **16**, 1824.
60 A. Bauzá, T. J. Mooibroek and A. Frontera, *Phys. Chem. Chem. Phys.*, 2014, **16**, 19192.
61 E. C. Escudero-Adán, A. Bauzá, A. Frontera and P. Ballester, *ChemPhysChem*, 2015, **16**, 2530.
62 A. Bauzá, T. J. Mooibroek and A. Frontera, *Chem. Rec.*, 2016, **16**, 473.
63 M. Servati Gargari, V. Stilinović, A. Bauzá, A. Frontera, P. McArdle, D. Van Derveer, S. W. Ng and G. Mahmoudi, *Chem. – Eur. J.*, 2015, **21**, 17951.
64 G. Mahmoudi, A. Bauzá and A. Frontera, *Dalton Trans.*, 2016, **45**, 4965.
65 G. Mahmoudi, A. Bauzá, M. Amini, E. Molins, J. T. Mague and A. Frontera, *Dalton Trans.*, 2016, **45**, 10708.
66 G. Mahmoudi, V. Stilinović, A. Bauzá, A. Frontera, A. Bartyzel, C. Ruiz-Pérez and A. M. Kirillov, *RSC Adv.*, 2016, **6**, 60385.
67 L. Shimoni-Livny, J. P. Glusker and C. W. Bock, *Inorg. Chem.*, 1998, **37**, 1853.
68 R. L. Davidovich, V. Stavila, D. V. Marinin, E. I. Voit and K. H. Whitmire, *Coord. Chem. Rev.*, 2009, **253**, 1316.
69 F. Yi-Min and T. Xi-Shi, *Acta Crystallogr., Sect. E: Struct. Rep. Online*, 2008, **64**, o65.
70 A. L. Gavrilova and B. Bosnich, *Chem. Rev.*, 2004, **104**, 349.
71 H. Hofmeier and U. S. Schubert, *Chem. Soc. Rev.*, 2004, **33**, 379.
72 G. te Velde, F. M. Bickelhaupt, E. J. Baerends, C. Fonseca Guerra, S. J. A. van Gisbergen, J. G. Snijders and T. Ziegler, *J. Comput. Chem.*, 2001, **22**, 931 and references therein.
73 E. J. Baerends, J. Autschbach, D. Bashford, A. Bérces, F. M. Bickelhaupt, C. Bo, P. M. Boerrigter, L. Cavallo, D. P. Chong, L. Deng, R. M. Dickson, D. E. Ellis, M. van Faassen, L. Fan, T. H. Fischer, C. Fonseca Guerra, A. Ghysels, A. Giammona, S. J. A. van Gisbergen, A. W. Götz, J. A. Groeneveld, O. V. Gritsenko, M. Grüning, F. E. Harris, P. van den Hoek, C. R. Jacob, H. Jacobsen, L. Jensen, G. van Kessel, F. Kootstra, M. V. Krykunov, E. van Lenthe, D. A. McCormack, A. Michalak, M. Mitoraj, J. Neugebauer, V. P. Nicu, L. Noodleman, V. P. Osinga, S. Patchkovskii, P. H. T. Philipsen, D. Post, C. C. Pye, W. Ravenek, J. I. Rodríguez, P. Ros, P. R. T. Schipper, G. Schreckenbach, M. Seth, J. G. Snijders, M. Solà, M. Swart, D. Swerhone, G. te Velde, P. Vernooijs, L. Versluis, L. Visscher, O. Visser, F. Wang, T. A. Wesolowski, E. M. van Wezenbeek, G. Wiesenekker, S. K. Wolff, T. K. Woo, A. L. Yakovlev and T. Ziegler, *ADF2012.01, Theoretical Chemistry*, Vrije Universiteit, Amsterdam.
74 T. van der Wijst, C. Fonseca Guerra, M. Swart, F. M. Bickelhaupt and B. Lippert, *Angew. Chem., Int. Ed.*, 2009, **48**, 3285.
75 C. Fonseca Guerra, T. van der Wijst, J. Poater, M. Swart and F. Matthias Bickelhaupt, *Theor. Chem. Acc.*, 2010, **125**, 245.
76 W. Gao, H. Feng, X. Xuan and L. Chen, *J. Mol. Model.*, 2012, **18**, 4577.
77 M. Mitoraj and A. Michalak, *J. Mol. Model.*, 2007, **13**, 347.
78 A. Michalak, M. Mitoraj and T. Ziegler, *J. Phys. Chem. A*, 2008, **112**, 1933.
79 M. Mitoraj, A. Michalak and T. Ziegler, *J. Chem. Theory Comput.*, 2009, **5**, 962.
80 A. Morsali, A. R. Mahjoub, S. J. Darzi and M. J. Soltanian, *Z. Anorg. Allg. Chem.*, 2003, **629**, 2596.
81 F. Marandi, B. Mirtamizdoust, S. Chantrapromma and H. K. Fun, *Z. Anorg. Allg. Chem.*, 2007, **633**, 1329.
82 F. Marandi, M. Mottaghi, G. Meyer and I. Pantenburg, *Z. Anorg. Allg. Chem.*, 2009, **635**, 165.
83 V. D. Schwade, E. Faoro and E. Schulz Lang, *Acta Crystallogr., Sect. C: Cryst. Struct. Commun.*, 2016, **72**, 525.
84 F. Caruso, M. L. Chan and M. Rossi, *Inorg. Chem.*, 1997, **36**, 3609.
85 S. Hino, M. Olmstead, A. D. Phillips, R. J. Wright and P. P. Power, *Inorg. Chem.*, 2004, **43**, 7346.
86 R. Echeverría, J. López-de-Luzuriaga, M. Monge and M. E. Olmos, *Chem. Sci.*, 2015, **6**, 2022.
87 A. Altomare, G. Cascarano, C. Giacovazzo and A. Guagliardi, *J. Appl. Crystallogr.*, 1993, **26**, 343.
88 G. M. Sheldrick, *Acta Crystallogr., Sect. A: Fundam. Crystallogr.*, 2008, **64**, 112.
89 C. F. Macrae, I. J. Bruno, J. A. Chisholm, P. R. Edgington, P. McCabe, E. Pidcock, L. Rodriguez-Monge, R. Taylor, J. van de Streek and P. A. Wood, *J. Appl. Crystallogr.*, 2008, **41**, 466.

